Modelling radar sea ice backscatter in support of the ERS-1 SAR

K.C. Partington and M. Hanna

GEC-Marconi Research Centre
West Hanningfield Rd., Great Baddow
Chelmsford, Essex CM2 8HN
UK

ABSTRACT

A model of radar backscatter from sea ice is presented together with results which are applicable to the configuration of the ERS-1 SAR. The model accounts for backscatter from the surface and volume of both sea ice and snow and is used as the basis for a sensitivity analysis to determine which parameters are most important in influencing the backscatter from sea ice. During winter, the model suggests that smooth multi-year ice is dominated by volume backscatter whilst first-year ice and possibly rough multi-year ice are dominated by surface backscatter, with negligible influence on backscatter caused by normal thicknesses of dry snow. During early summer, the presence of a moist snow layer over the ice can cause the ice backscatter to be attenuated at very low moisture contents but, depending on surface roughness, the backscatter then rises as a result of dominance by the snow surface. The exact behaviour in summer is very sensitive to both surface roughness and snow moisture conditions, with first-year ice generally exhibiting increased backscatter whilst multi-year ice generally shows reduced backscatter. The results of the modelling are coarsely validated using published backscatter measurements obtained from published campaign results.

1. INTRODUCTION

The advent of ERS-1 and the promise of a near-continuous satellite radar monitoring capability over the next decade or more has prompted movement towards the development of a number of SAR image analysis systems capable of aiding operations in polar waters. The attraction to polar operators of such systems is clear. Sea ice presents a hazard to shipping and geophysical survey and rig operations which not only influences efficiency of operations but presents severe technical challenges to design studies. Synthetic Aperture Radar (SAR) is able to monitor the surface in virtually all weather conditions and during night as well as day. As a means of providing a high resolution monitoring capability over areas of the order of 10 000 km^2, the SAR is unrivalled.

One of the key parameters of interest to operators is the type of sea ice. This parameter, expressed as ice type concentration or as a map combined with motion information, can be used by an operator to determine whether routeing in an area is possible. Knowledge of the prevalence of ice types in particular areas can be used to assess the technical requirements associated with hydrocarbon extraction in that area. One of the main requirements of an image analysis system is therefore to distinguish between different types of sea ice. To achieve this it is necessary to understand the interaction of the radiation with the different types of sea ice. The types of sea ice of primary interest to operators are first-year ice and multi-year ice.

This paper addresses the problem of distinguishing between these two types of ice, and open water. In contrast to previous papers, this paper investigates the specific case of detection at the configuration of the ERS-1 SAR, and presents results which distinguish between the different scattering mechanisms. The model also treats the sea ice as a mixture of needle-like as well as spherical scattering elements, in line with observations on the form of brine inclusions. Results are provided for both winter and early summer conditions.

2. MODELLING BACKSCATTER FROM SEA ICE

To investigate the scattering mechanisms and contrasts of type of sea ice and open water, it is necessary to supplement observations with modelling. Whilst observations can provide insight into contrasts, it is only through undertaking modelling that the underlying scattering processes can be determined. Here, a model is used to investigate the

(normalised) backscatter coefficient from sea ice and the predictions are compared with observations derived from published results of campaigns.

2.1 Scattering Model

The backscatter from the sea ice is assumed to consist of scatter from a layer of snow and the underlying sea ice (Figure 1). The general model is as follows:

$$\sigma^0 = \sigma^0_{ss} + \sigma^0_{sv} + \sigma^0_{is} + \sigma^0_{iv} \quad (1)$$

where is σ^0 the scattering coefficient and
σ^0_{ss} = snow surface component;
σ^0_{sv} = snow volume component;
σ^0_{is} = ice surface component;
σ^0_{iv} = ice volume component.

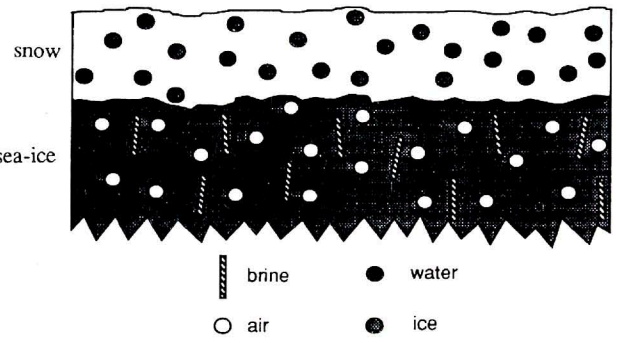

Fig. 1 - Illustration of the model of sea ice, showing snow and ice layers and inclusions

In the following equations, other parameters are defined as follows:
N = volume density of scatterers (subscript i for ice, b for brine, a for air and w for water);
T = transmission coefficient (subscript as and si indicate air/snow and snow/ice interfaces respectively, with 1 indicating transmission down and 2 indicating transmission up);
β = extinction coefficient (subscript s indicating snow and si indicating sea ice);
θ = local angle of incidence, with refraction effect (θ') in the first layer and in the second layer (θ'');
d = depth of medium (subscript s indicates snow and i indicates ice).

The backscatter from the snow surface (σ^0_{ss}) is treated using a classical scattering theory (Ulaby *et al.*, 1986, Chapter 12), and it is assumed that the snow surface roughness has similar characteristics to the underlying ice surface (this is necessary in the absence of independent information on snow surface roughness).

σ^0_{sv} is predicted using a combination of scattering from ice and water particles, both treated as Rayleigh scattering sources, with the backscatter attenuated by passage through the snow layer, as follows:

$$\sigma^0_{sv} = (N_i \langle |f_{svi}|^2 \rangle + N_w \langle |f_{svw}|^2 \rangle)\, T_{as1}\, T_{as2} \left(\frac{1 - \exp(-2\beta_s d_s / \cos\theta')}{2\beta_s / \cos\theta'} \right) \quad (2)$$

Here, the first term is the VV component of the total phase matrix for the snow layer, including the scattering amplitudes for ice and water particles (f_{svi} and f_{svw}). The extinction coefficient is calculated by combining the absorption coefficient and the scattering coefficient for moist snow, assuming Rayleigh scatterers, using the procedure described by Ulaby *et al.* (1986, p. 1603-6), where scattering is assumed to be caused by ice particles and the effect of the water is to influence the dielectric constant of the background material (water and air) which influences the absorption coefficient. The transmission coefficient is calculated using the bistatic scattering coefficients from the classical scattering theories (Ulaby *et al.*, 1986, Chapter 12).

The backscatter from the sea ice surface is calculated as follows:

$$\sigma^0_{is} = \sigma^0_{is1}\, T_{as1}\, T_{as2} \exp(-2\beta_s d_s / \cos\theta') \quad (3)$$

where σ^0_{is1} is the backscatter from the ice-snow interface, with the dielectric discontinuity calculated accordingly. Again, a classical surface scattering theory is used (Ulaby *et al.*, 1986, Chapter 12).

The backscatter from the ice volume is the last element in the model. It is calculated using the following equation:

$$\sigma^0_{iv} = (N_b \langle |f_{ivb}|^2 \rangle + N_a \langle |f_{iva}|^2 \rangle)\, T_{as1}\, T_{as2}\, T_{si1}\, T_{si2} \left(\frac{1 - \exp(-2\beta_i d_i / \cos\theta'')}{2\beta_i d_i / \cos\theta''} \right) \exp(-2\beta_s d_s / \cos\theta') \quad (4)$$

where f_{ivb} is the scattering amplitude associated with a brine inclusion and f_{iva} is the scattering amplitude associated with an air bubble.

Volume scattering from the sea ice is calculated using a model for needles of brine and spheres of air embedded in fresh ice. The spheres are Rayleigh scatterers, with radius

much less than that of the wavelength, but the needles are only required to be small compared to the wavelength in one dimension. This is the approach reported by Schiffer and Thielheim (1979) and Lang and Saleh (1985) for simply-shaped particles, and is essentially a 'lossy scatterer' model. Analytic expressions for the backscatter from particles are obtained by assuming that the field is constant across one dimension of the particle. Other assumptions of the model include the requirement of a sparse distribution of scatterers so that scattering is in the far-field and the assumption of no scattering from the base of the sea ice, which is probably acceptable given the penetration depths of sea ice. The brine needles have an inclination probability distribution which is assumed to be Gaussian, with the mean and standard deviation being specified. This allows the needles to be located with a predominantly vertical orientation. Otherwise, the distribution of all scatterers is assumed to be random. The average backscatter coefficient is integrated until the estimate converges towards a mean value with variation of less than 2%.

2.2. Dielectric Model

The bulk dielectric constant for the sea ice is calculated using a mixing model. The mixing model estimates the bulk dielectric constant for a two-phase mixture, so it must be used iteratively, twice, in order to derive the dielectric constant of a three-constituent mixture such as sea ice. For the first iteration, the dielectric constant for a mixture of brine and pure ice is estimated. For the second iteration, air inclusions are added. For snow an analogous procedure is undertaken, but in the first case the dielectric constant is derived for a water cloud and in the second iteration the dielectric constant for ice particles within this cloud is calculated.

The mixing model is as follows (de Loor, 1968):

$$\varepsilon_m = \varepsilon_h + \frac{1}{3} \sum_{u=a,b,c} \frac{\vartheta_i(\varepsilon_i - \varepsilon_h)}{1 + A_u(\varepsilon_i/\varepsilon^* - 1)} \qquad (5)$$

where ε is the (complex) dielectric constant; subscripts m, h and i represent the mixture, host and inclusion material respectively; a, b and c are the axes associated with the inclusion and u is the axis which is oriented parallel to the applied field. Also, ε^* is the dielectric constant of the material immediately surrounding the inclusion. For small values of υ_i, the inclusion volume fraction (<0.1), short range particle interactions may be assumed to be negligible in which case ε^* is taken to be equal to ε_h. A_u is the depolarisation factor of an ellipsoid along its u axis (u=a, b or c). An expression for A_u can be calculated under the assumption of a more specific shape for the inclusion, including spheres and needles which are of particular interest here and expressions for the bulk dielectric constant when the field is aligned along each of the axes of the inclusion are given explicitly in equation (6).

ε_m spheres

$$\varepsilon_h\left[1 + \frac{3\vartheta_i(\varepsilon_i - \varepsilon_h)}{(\varepsilon_i + 2\varepsilon_h)}\right]^{\varepsilon_m^a} \quad \varepsilon_h\left[1 + \frac{3\vartheta_i(\varepsilon_i - \varepsilon_h)}{(\varepsilon_i + 2\varepsilon_h)}\right]^{\varepsilon_m^b} \quad \varepsilon_h\left[1 + \frac{3\vartheta_i(\varepsilon_i - \varepsilon_h)}{(\varepsilon_i + 2\varepsilon_h)}\right]^{\varepsilon_m^c}$$

ε_m needles

$$\varepsilon_h\left[1 + \frac{2\vartheta_i(\varepsilon_i - \varepsilon_h)}{(\varepsilon_i + 2\varepsilon_h)}\right] \quad \varepsilon_h\left[1 + \frac{2\vartheta_i(\varepsilon_i - \varepsilon_h)}{(\varepsilon_i + 2\varepsilon_h)}\right] \quad \varepsilon_h + \vartheta_i(\varepsilon_i - \varepsilon_h) \qquad (6)$$

In general, the applied field is not directed along one of the axes of the inclusion and it is necessary to calculate the dielectric constant resulting from a more general orientation and inclination of inclusions. This can be calculated using the following expression (Ulaby *et al.*, 1986, Vol. 3):

$$e_m = \frac{\varepsilon_m^b + \varepsilon_m^\gamma}{2}$$

$$\varepsilon_m^\gamma = \left(\frac{\sin^2\gamma}{\varepsilon_m^a} + \frac{\cos^2\gamma}{\varepsilon_m^b}\right)^{-1} \qquad (7)$$

where ε_m is the dielectric constant associated with the mixture; the superscripts a and b refer to the axes consistent with equation 6 and the superscript γ is an arbitrary angle. It is useful to keep the generality associated with equation 7 and it is possible to calculate the dielectric constant numerically using suitable distributions for the orientation and inclination angle of the inclusions, consistent with the model of volume scattering and this is the procedure used in this paper. The orientation angle distribution is taken to be uniform whilst the inclination angle distribution is taken to be Gaussian, with the mean and standard deviation specified as appropriate. Vant *et al.* (1978) found that the most appropriate fit to data was obtained when the angular distribution of inclusions was between 35° and 45° to the normal for vertically-directed radiation.

For snow, equation (5) is also used but the depolarisation factors given by A_a, A_b and A_c for calculating the dielectric constant of the air-water mixture are given as 0.88, 0.06 and 0.06 by Ambach and Denoth (1980). This is because the water particles are non-spherical. To calculate

ε_m in this case it is necessary to solve (5) by iteration. The ice particles are assumed to be spherical so the second iteration is straightforward. The dielectric model for damp snow should strictly be adjusted according to whether the water is held in the pendular or funicular regime (Drinkwater, 1989). In this paper, we will consider only low levels of moisture content appropriate to the pendular regime.

The parameters which must be known in order for the mixing model to be used are the dielectric constants and volume fractions of water, brine and pure ice. The dielectric constant of water is assumed to be (65.81-36.51j). The dielectric constant of brine is calculated using Stogryn's (1971) Debye form for the dielectric constant, which is semi-empirical and requires as input only the temperature of the brine and radiation frequency. The volume fraction of brine is calculated from the salinity of the sea ice and its temperature (Ulaby *et al.*, 1986, Vol. 3). The dielectric constant of pure ice is also assumed to follow a Debye form, but whilst the real part is almost constant in the microwave range, the loss has proved to be rather difficult to predict using a semi-theoretical model. For this reason, an empirical equation is used based on experimental data from Evans (1965), Lamb (1946) and Lamb and Turney (1949) for frequencies (f) between 1 and 10 GHz, as follows:

$$\log_{10}\lfloor f\,10^3 \tan\delta\rfloor = A_0 + A_1 \log_{10} f \qquad (8)$$

where A_0 and A_1 are dependent only on temperature. The predictions from these models are illustrated in Figures 2 and 3 for sea ice and snow respectively.

2.3. Volume Scattering

The backscatter from the volume of the sea ice and snow is from the inclusions, which may be either air, water, ice or brine. The expressions for snow and ice respectively are as follows:

$$\begin{aligned}\langle\sigma^0_{sv}\rangle &= N_i\langle|f_i|^2\rangle + N_w\langle|f_w|^2\rangle\\ \langle\sigma^0_{iv}\rangle &= N_a\langle|f_a|^2\rangle + N_b\langle|f_b|^2\rangle\end{aligned} \qquad (9)$$

The scattered field, $\langle|f_x|^2\rangle$, can be modelled using a "lossy scatterer model", as follows (Ishimaru, 1978, eq. 2-27; Lang and Saleh, 1985, eq. 4; Schiffer and Thielheim, 1979, eq. 9, 13-15):

$$\langle|f_x|^2 = \frac{k_i^4\,V^{inc2}}{16\pi^2}\int_0^{2\pi}\int_{-\infty}^{\infty}\left|\left\{A^{inc}(\bar{\alpha}_i.\bar{\alpha}_o) + B^{inc}(\bar{n}^{inc}.\bar{\alpha}_i)(\bar{n}^{inc}.\bar{\alpha}_o)\right\}Q^{inc}\right|^2 d\theta_p\,d\phi \qquad (10)$$

where subscript x indicates one of ice, water, brine and air (i,w,b,a), V^{inc} is the volume of the particle, α_o and α_i are the polarisation vectors associated with the transmitted and backscattered field, k_i is the wavenumber inside the medium, n^{inc} is the vector associated with the orientation and inclination of the major axis of the inclusion and A^{inc}, B^{inc} and Q^{inc} are defined as follows (needles for brine, Schiffer and Thielheim, 1979; spheres for air, ice and water, Stratton, 1941):

	A^{inc}	B^{inc}	Q^{inc}
needles	$\frac{2\chi}{\chi+2}$	$\frac{\chi^2}{\chi+2}$	$\frac{\sin\{k_i a(\cos\theta_i\cos\theta_p + \cos\phi\sin\theta_i\sin\theta_p)\}}{\{k_i a(\cos\theta_i\cos\theta_p + \cos\phi\sin\theta_i\sin\theta_p)\}}$
spheres	$\frac{3\chi}{\chi+3}$	0	1

Here, a is the length of the needle and $\chi = (\varepsilon_i - \varepsilon_h)/\varepsilon_h$. The various vectors are defined as follows:

$$\bar{\alpha}_i = \begin{bmatrix}\cos\theta_i'\\ 0\\ -\sin\theta_i'\end{bmatrix} \qquad \bar{\alpha}_o = \begin{bmatrix}\cos\theta_i'\\ 0\\ -\sin\theta_i'\end{bmatrix} \qquad \bar{n}^{inc} = \begin{bmatrix}\cos\phi\sin\phi_p\\ \sin\phi\sin\phi_p\\ \cos\phi_p\end{bmatrix}$$

Here, θ'_i is the angle of refraction and the polarisation vectors are defined for the vertical polarisation case. The backscattered amplitude from a single inclusion must undergo attenuation as it travels through the medium. This is calculated through the following equation for a single type of inclusion:

$$\beta_x = N^{inc}k_i V^{inc}\int_0^{2\pi}\int_{-\infty}^{\infty}\mathrm{Imag}\left\{A^{inc}(\bar{\alpha}_i.\bar{\alpha}_o) + B^{inc}(\bar{n}^{inc}.\bar{\alpha}_i)(\bar{n}^{inc}.\bar{\alpha}_o)\right\}Q^{inc}\,d\theta_p\,d\phi \qquad (11)$$

where x indicates air, ice, water or brine, N^{inc} is the number density of inclusions and the scattering amplitudes are evaluated in the forward direction. The total extinction coefficient is then calculated by adding the extinction due to the types of inclusion present within the medium. Thus:

$$\begin{aligned}&\beta_s = \beta_i + \beta_w\\ &\text{and}\\ &\beta_{si} = \beta_b + \beta_a\end{aligned} \qquad (12)$$

The integrals can be calculated numerically. It is assumed here that the orientation angle distribution (over angle ϕ) is uniform between 0 and 2π. It is also assumed that the inclination angle distribution is Gaussian.

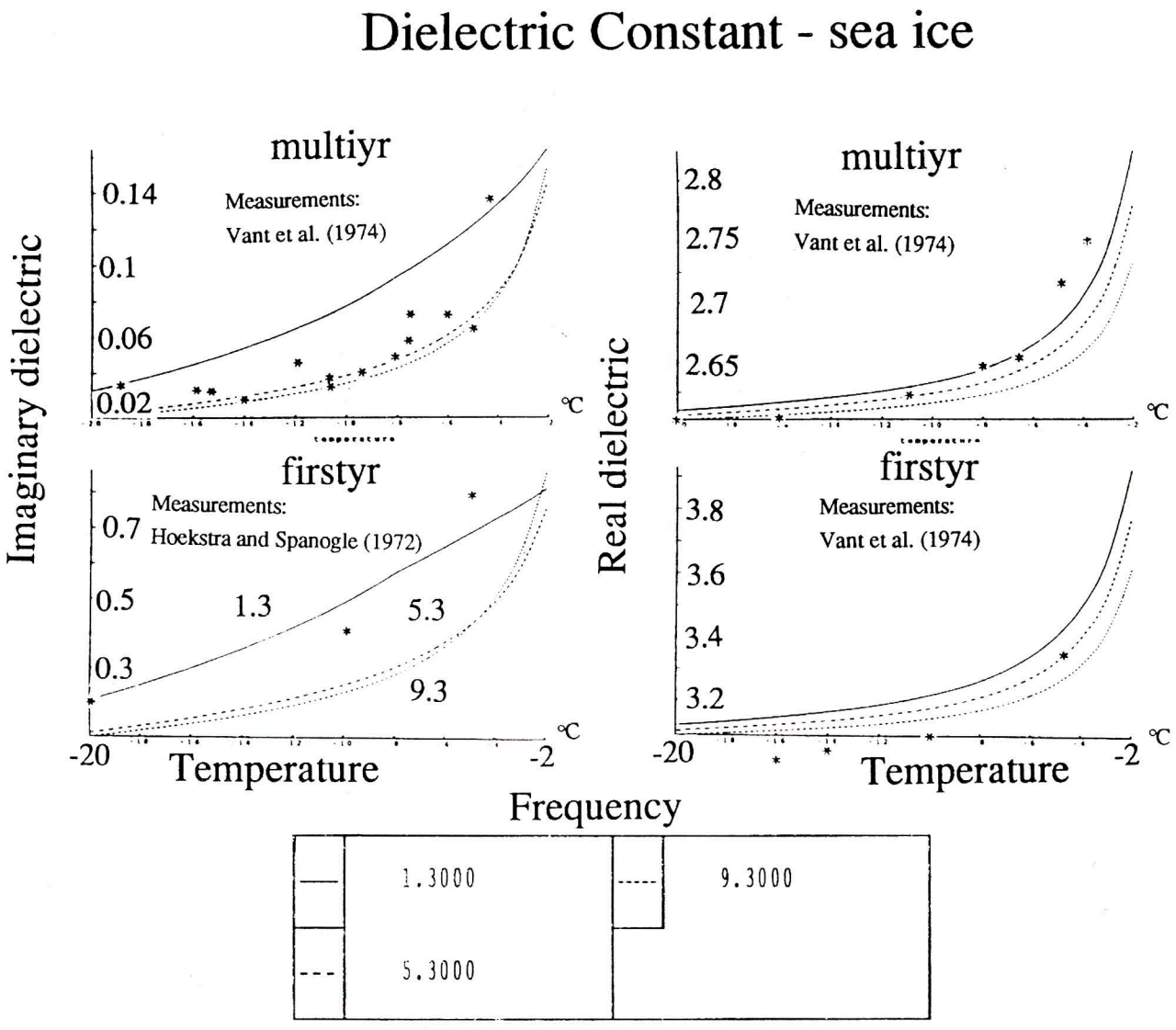

Fig. 2 - Predicted and measured dielectric constant of sea ice. (a) top left - multi-year sea ice, imaginary dielectric constant; (b) top right - multi-year sea ice, real dielectric constant; (c) bottom left - first-year sea ice, imaginary dielectric constant and (d) bottom right - first-year sea ice real dielectric constant. Measurements from Vant et al. (1974) and Hoekstra and Spanogle (1972). First-year ice salinity is 5.0 ‰ and multi-year ice salinity is 0.6‰

2.4. Surface Scattering

Surface scattering is treated using the Kirchhoff Scalar Approximation model, attenuated in the case of sea ice by passage through the overlying snow. Figure 4 suggests that this is acceptable for most measurements of the surface roughness characteristics of sea ice. Insufficient information is available on differences in surface roughness between multi-year and first-year ice and so the same range of surface roughness is used for both, as is the case for the snow and sea ice surfaces also. From Figure 4, it can be seen that a range of roughness characteristics are covered by a correlation length of 0.08 m and height standard deviations ranging from 0.001 to 0.016 m. This range is used to model the variation in backscatter from snow and ice surfaces.

3. MODELLING RESULTS

The model described above has been used to predict backscatter from first-year and multi-year sea ice using the parameters described in Table 1, which indicates default values with ranges shown in brackets. The values in Table 1 are obtained from a survey of the literature for sea ice characteristics. A sensitivity analysis was undertaken for all parameters and the differences in backscatter between ice types were analysed together with the dominant scattering mechanisms.

For crude comparison with the predictions, a survey of measurements of backscatter at the configuration of the

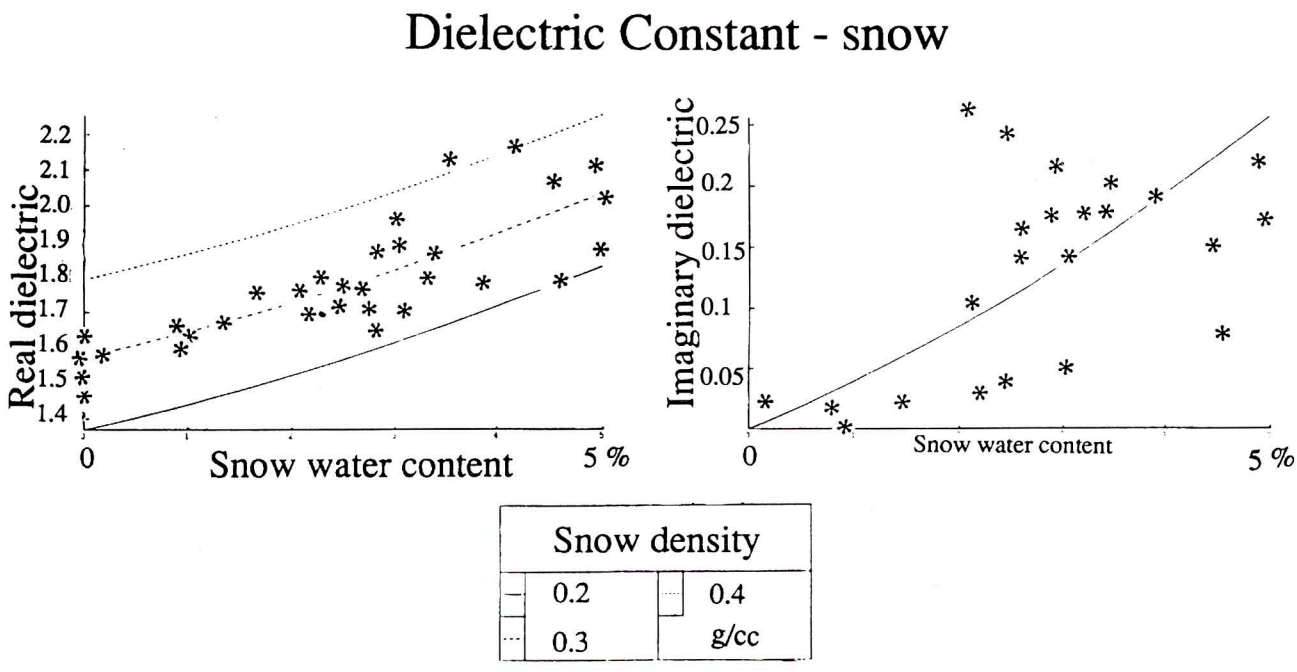

Fig. 3 - Predicted and measured dielectric constant of snow. Top (a) real dielectric constant and bottom (b) imaginary dielectric constant. Measurements from Hallikainen et al. (1986)

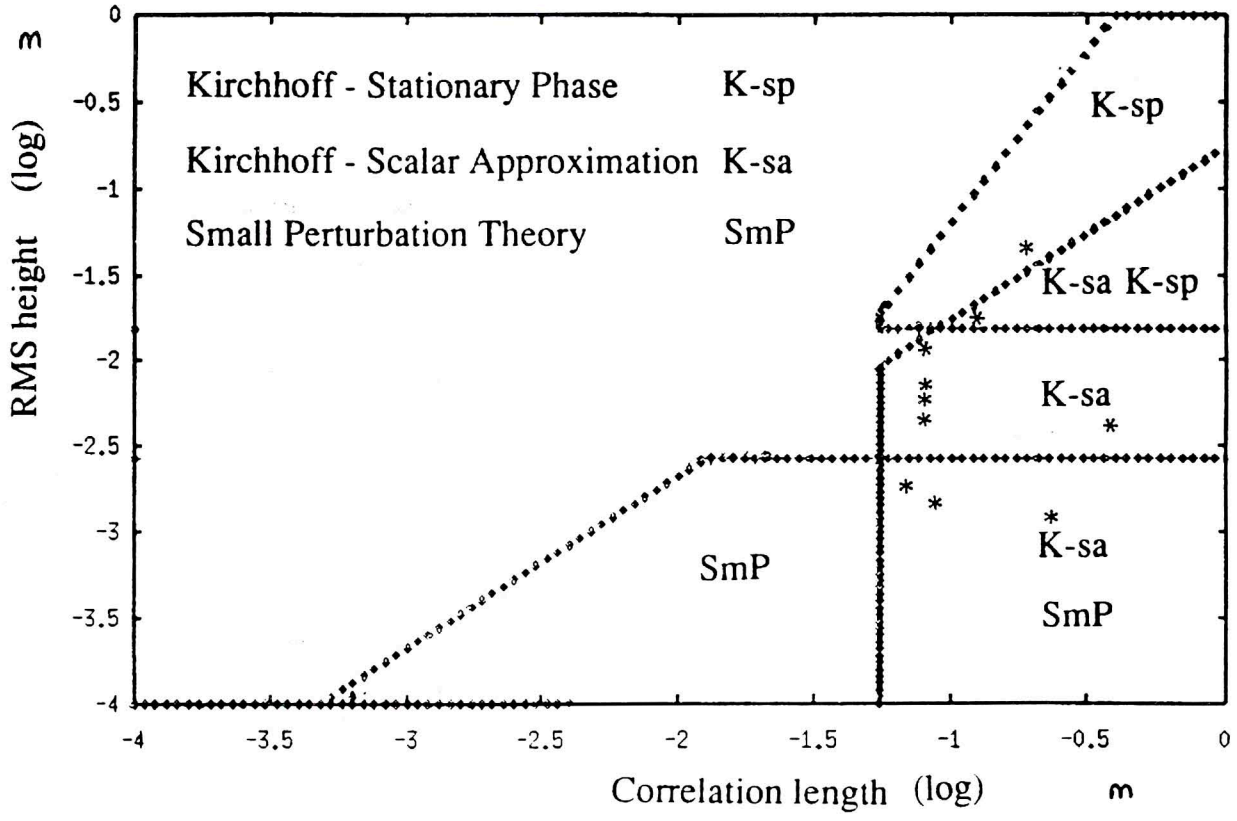

Fig. 4 - Surface backscatter model limits of applicability for ERS-1, together with measurements from Drinkwater (1989), Livingstone and Drinkwater (1991), Ulander and Carlstrom (1992) and Kim et al. (1984)

Table 1 - Default and ranges of parameters for sea ice backscatter modelling

	first-year ice	multi-year ice
temperature	-14°C (-30.0 to -5)	-14°C (-30.0 to -5)
density	0.88 g/cc (0.85 to 0.92)	0.70 g/cc (0.65 to 0.75)
salinity	5.0 ‰ (1.0 to 9.0)	0.6 ‰ (0.1 to 1.1)
brine needle radius	0.000025 m	0.000025 m
brine needle length	0.025 m (0.000025 to 0.025)	0.025 m
air bubble radius	0.00075 m	0.002 m (0.001 to 0.003)
rms height	0.0015 m (0.001 to 0.018)	0.0015 m (0.001 to 0.018)
correlation length	0.08 m	0.08 m
snow density	0.25 g/cc (0.25 to 0.50)	0.25 g/cc (0.25 to 0.50)
snow depth	0.10 m (0.0 to 0.20)	0.10 m (0.0 to 0.50)
snow water content	0.0 and 0.3 (0.0 to 0.15)	0.0 and 0.3 (0.0 to 0.15)
snow rms height	0.0015 m (0.001 to 0.018)	0.0015 m (0.001 to 0.018)
snow correlation length	0.08 m	0.08 m
snow ice particle size	0.001 (0.0005 to 0.0015)	0.001 (0.0005 to 0.0015)

ERS-1 SAR was undertaken and the results are summarised in Figure 5. In all subsequent comparisons of measurements with predictions, crude normalised frequency curves for backscatter measurements are generated from the categories of FY_{sm} (smooth first-year ice) and MY (multi-year ice) based on these reported measurements.

3.1 Winter Backscatter Predictions

The results of the analysis of backscatter under cold winter conditions are shown in Figure 6 and 7. For smooth first-year ice the model predicts quite well the mean backscatter, but the range of values is under-predicted when only the volume components of the ice are considered (Figure 6a). This is because there is no significant volume scattering from the first-year ice and it is necessary to consider surface roughness in order to predict more realistically the range of backscatter from first-year ice. It may also be a result of not including any variation in the air bubble size in first-year ice. The range of backscatter values is predicted quite well using the range of surface roughness parameters given in Section 2.4. Dry snow is predicted to have no effect on the backscatter from sea ice for typical depths, although this may not be true of backscatter from the smoothest first-year floes.

Figure 7 shows a similar pair of graphs for multi-year sea ice. Again, the mean backscatter is predicted quite well, using just volume scattering. The range of recorded backscatter values is much smaller than for first-year ice and this may indicate that the backscatter is less sensitive to variations in surface roughness. It may also indicate that the range of surface roughness values of multi-year ice is less than for first-year ice. However, the model predicts that the backscatter from multi-year ice is dominated by volume scattering except for the highest rms surface roughness values used. The model also predicts that the variations in backscatter are caused mainly by variations in air bubble diameter. All other parameters, such as density and salinity are less important. Figure 7b shows the predicted surface scattering from multi-year ice. The range of values is similar to those predicted for first-year ice as the same range of surface roughness values are used and the differences in dielectric constant for the two ice types do not have much effect on surface scattering. Surface scattering is generally less important than volume scattering in the case of multi-year ice.

The contrast in backscatter from both smooth first-year ice and multi-year ice is predicted and measured to be of the order of 6 or 7 dB in the mean, but the range of contrasts is indicated to be extremely large, with no contrast predicted at one end of the scale. However, occurrences of no contrast between ice types is predicted and measured to be very rare. Thus, during winter it may be expected that contrast between ice types will usually be sufficient to be calculated from mean backscatter alone.

3.2. Early Summer Conditions

Predictions of backscatter from first-year and multi-year ice have been made for conditions during summer when

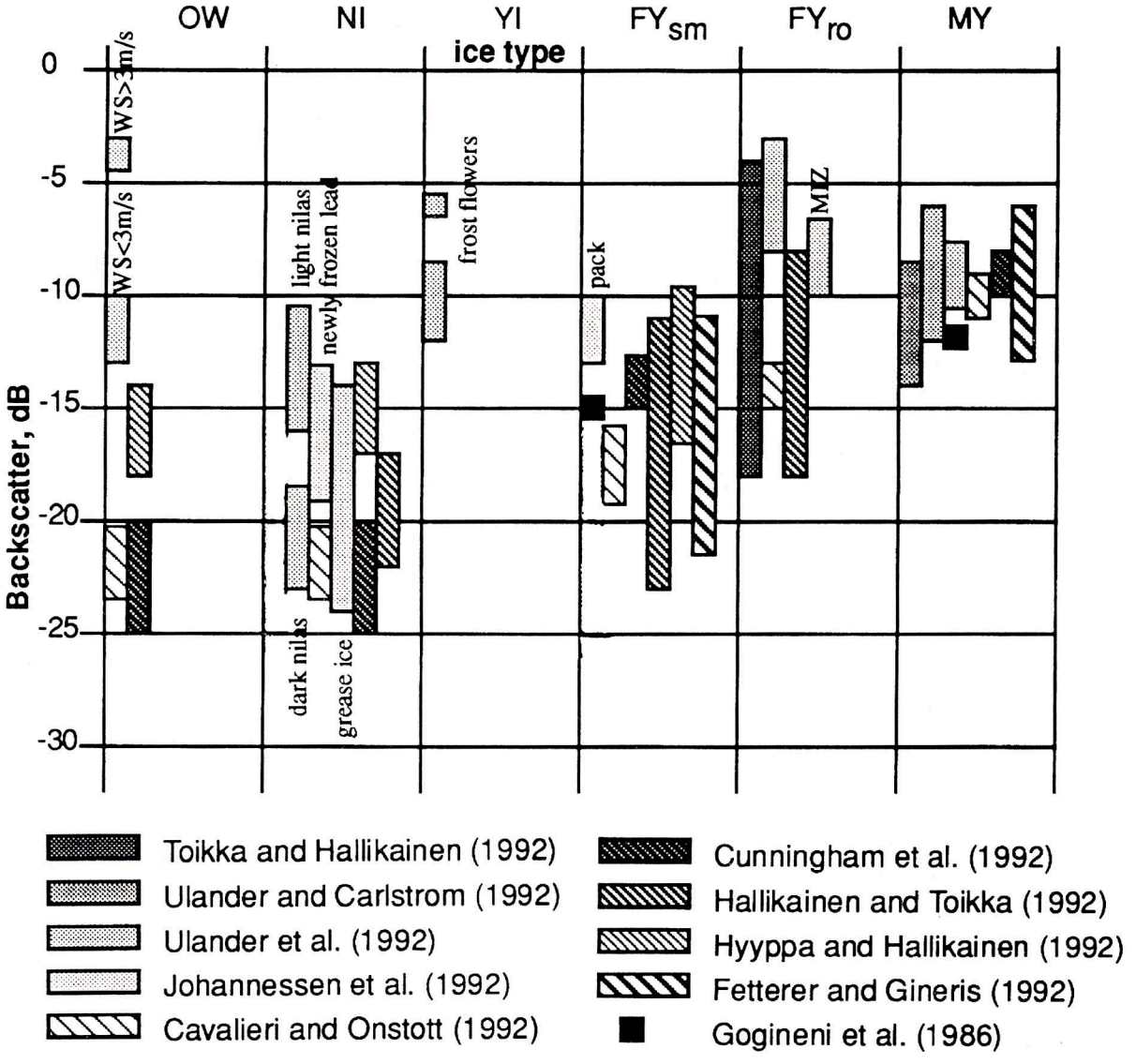

OW = open water
NI = new ice
YI = young ice
FY_{sm} = first year (smooth) ice
FY_{ro} = first year (rough) ice
MY = multi year ice

Fig. 5 - Measurements of the (normalised) backscatter coefficient from sea ice at the configuration of the ERS-1 SAR obtained from the literature. All measurements are for the winter period

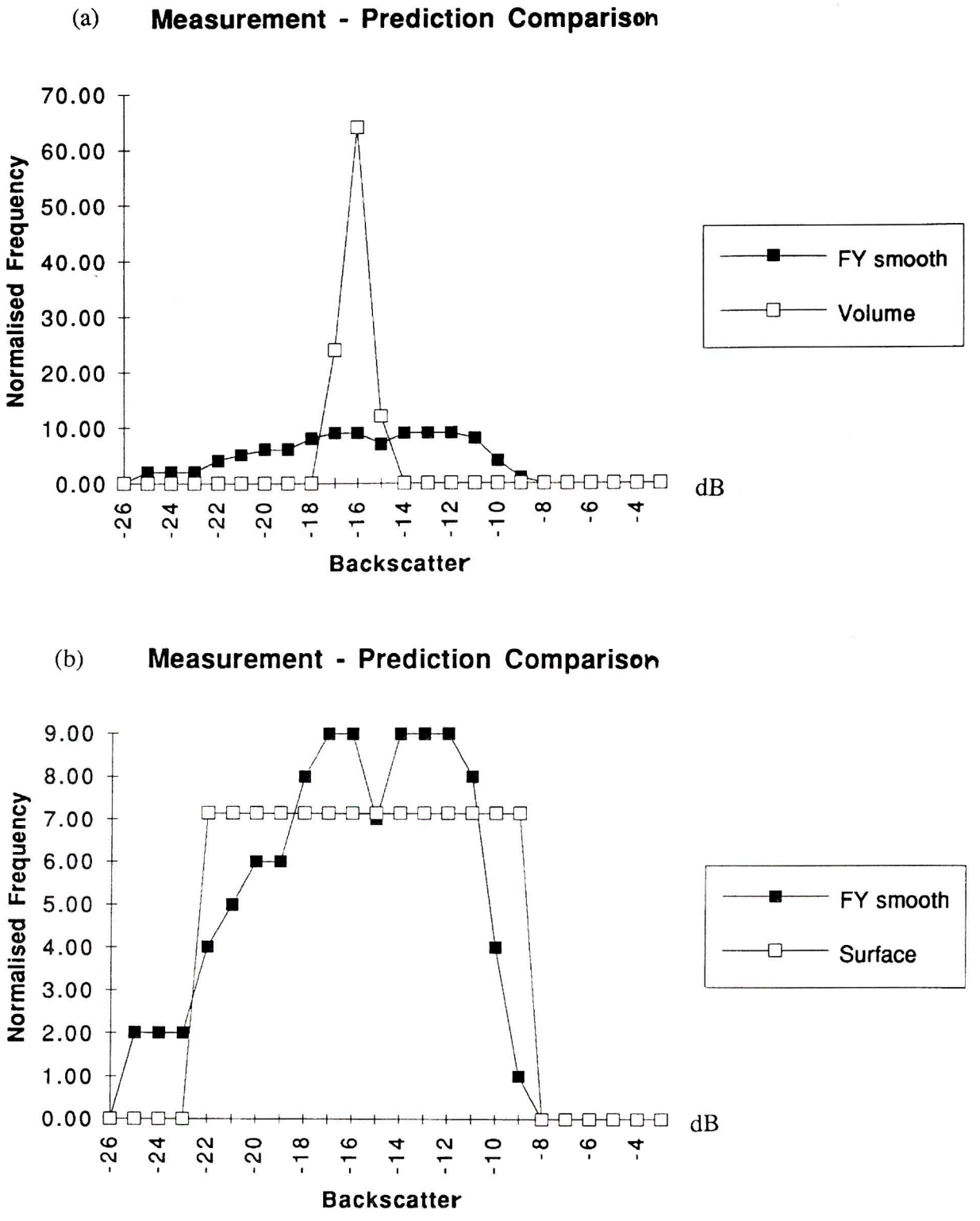

Fig. 6 - Predictions of the backscatter coefficient in dB for smooth winter first-year ice as a function of (top - a) volume parameters (brine radius, density, etc.) and (bottom - b) surface roughness. Also shown is the crude normalised frequency of measurements obtained from Figure 5 for smooth first-year ice (normalised frequency being defined as the area under the frequency curve being 100)

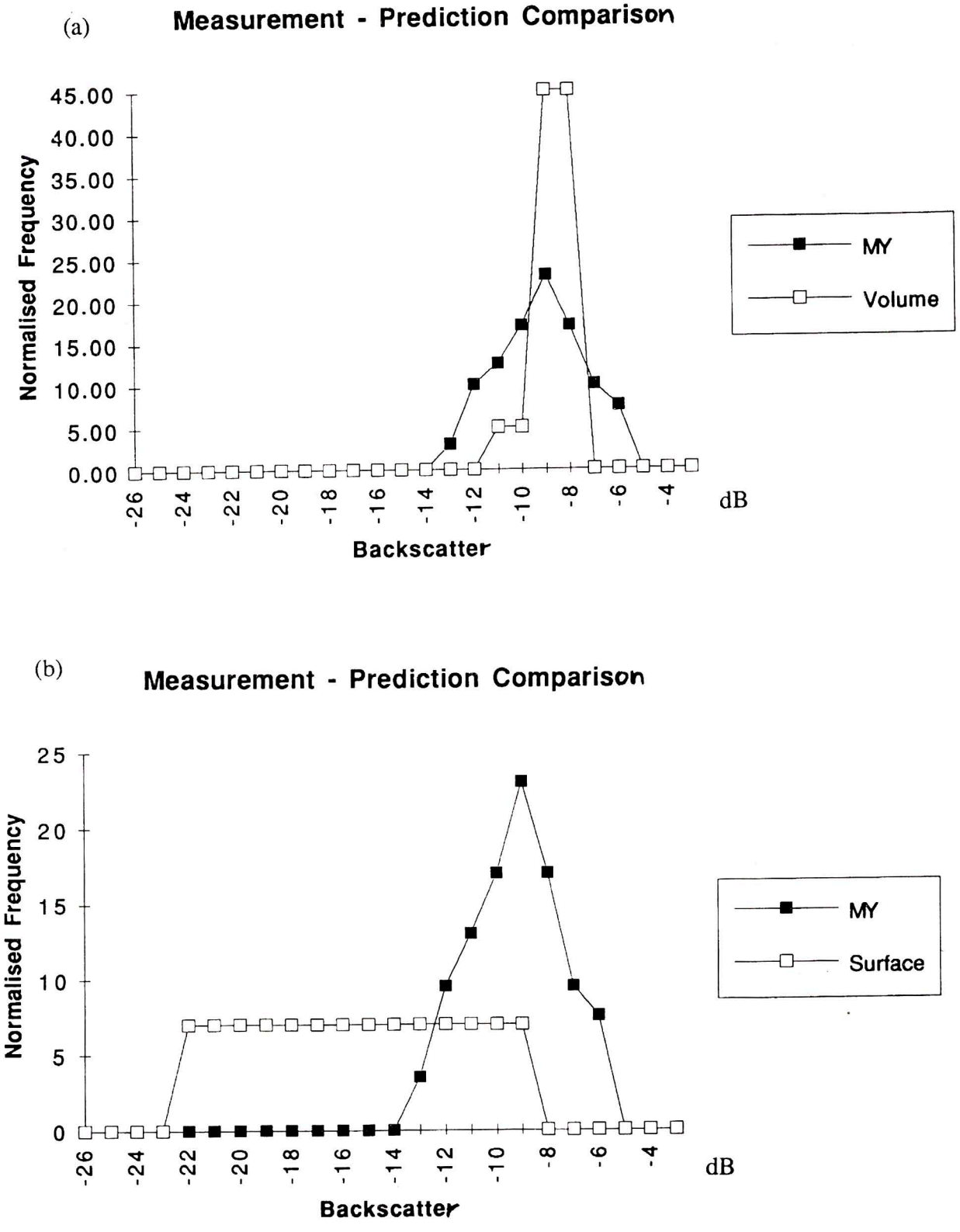

Fig. 7 - Predictions of the backscatter coefficient in dB for winter multi-year ice as a function of (top - a) volume parameters (air bubble radius, density, etc.) and (bottom - b) surface roughness. Also shown is the crude normalised frequency of measurements obtained from Figure 5 for multi-year ice (normalised frequency being defined as the area under the frequency curve being 100)

the snow layer is damp and the underlying ice remains cold and dry. This does not represent summer conditions generally, but it provides an indication of conditions during the early part of summer.

Figure 8 shows predictions for backscatter from the ice and snow surfaces and volumes during these conditions. Figure 8a and 8b show conditions for first-year and multi-year ice with a slightly rough snow surface, with backscatter from the surface at its lowest level in the range given and Figure 8c and 8d show similar graphs for moderately rough snow surfaces. It can be seen that for first-year ice, low levels of snow wetness can attenuate the return from the ice surface and so actually reduce backscatter for a time, but that this only happens with the smoother snow surface. For both roughnesses, the backscatter for first-year ice increases at higher levels of snow wetness as a result of the snow surface becoming an important scattering element. For multi-year ice the situation is different. As the backscatter from multi-year ice without snow is greater, in general than for first-year ice, the main effect of the damp snow layer is to attenuate the return from the ice and so the backscatter is more likely to be reduced for multi-year ice. Again, at very high levels of snow wetness and roughness the backscatter may be larger than for the ice alone but this is considered likely to be unusual.

The reversal of backscatter contrast (as opposed to the extinction of contrast) is not predicted using this model as the same snow characteristics are used for both first-year and multi-year ice. However, if the differences between first-year and multi-year ice at any one time are considered then it is possible to understand how the backscatter from the multi-year ice is reduced to below that of first-year ice. If there is less snow on first-year ice and it melts before the snow on multi-year ice, then a layer of superimposed ice may be exposed on the first-year ice thus making the backscatter larger than from multi-year ice (Onstott et al., 1987).

5. OPEN WATER

In addition to distinguishing first-year ice from multi-year ice, it is important to be able to distinguish both these ice types from open water. Figure 9 shows predictions of the CMOD4 model of backscatter from open water provided by Lecomte (1993). It can be seen that, for wind speeds greater than about 5 m/s, backscatter from open water will be expected to be greater than that from most ice types. To predict such backscatter accurately will require information not only on wind speed but also on wind direction. Onstott (personal communication, 1993) reports that cases of the backscatter from open water overlapping with backscatter from ice (other than new ice) are comparatively rare and the Alaskan SAR Facility uses this to classify the surface as open water / new ice if the backscatter falls below or above that of thresholds provided for ice types (which are assumed to be insensitive to wind speed).

Figure 9 also shows that the range of incidence angles associated with an ERS-1 image is sufficiently large to cause the backscatter from open water to vary significantly across the image. Fortunately, this variation (in dBs) appears to be approximately linear over this range of angles and appears to be relatively insensitive to wind speed and so this may be used in the discrimination of open water from ice.

6. CONCLUSIONS

A backscatter model for snow-covered sea ice has been presented which broadly succeeds in predicting measurements from ERS-1 SAR sea ice data. The backscatter from multi-year ice is less variable than from first-year ice, this being predicted to be a result of backscatter from multi-year ice being more dependent on volume scattering than surface scattering. Rough first-year ice has a similar level of backscatter to multi-year ice, but it is likely that the scattering mechanism for this is largely surface scattering. For polar operators, it is more important to classify rough first-year ice with multi-year ice than to mis-classify multi-year ice as first-year ice and so the threshold for classification of multi-year ice should be kept low rather than high.

In early summer, the backscatter contrast from ice types can disappear or reverse and it is important under these circumstances to make use of texture and shape in classifying ice type. Differences in texture caused, for example, by differences in multi-year and first-year ice ridge signatures, may help in distinguishing ice type in these circumstances. With a damp snow cover, the backscatter from multi-year ice can be reduced by many dBs as a result of suppression of backscatter from the ice volume and surface whilst the backscatter from first-year ice can be enhanced by the backscatter from damp snow being greater than the backscatter from bare ice.

Open water shows a wide range of backscatter values but for wind speeds greater than about 5 m/s open water is brighter than the ice. In general, areas of open water will appear as brighter or darker than the ice. In the case of

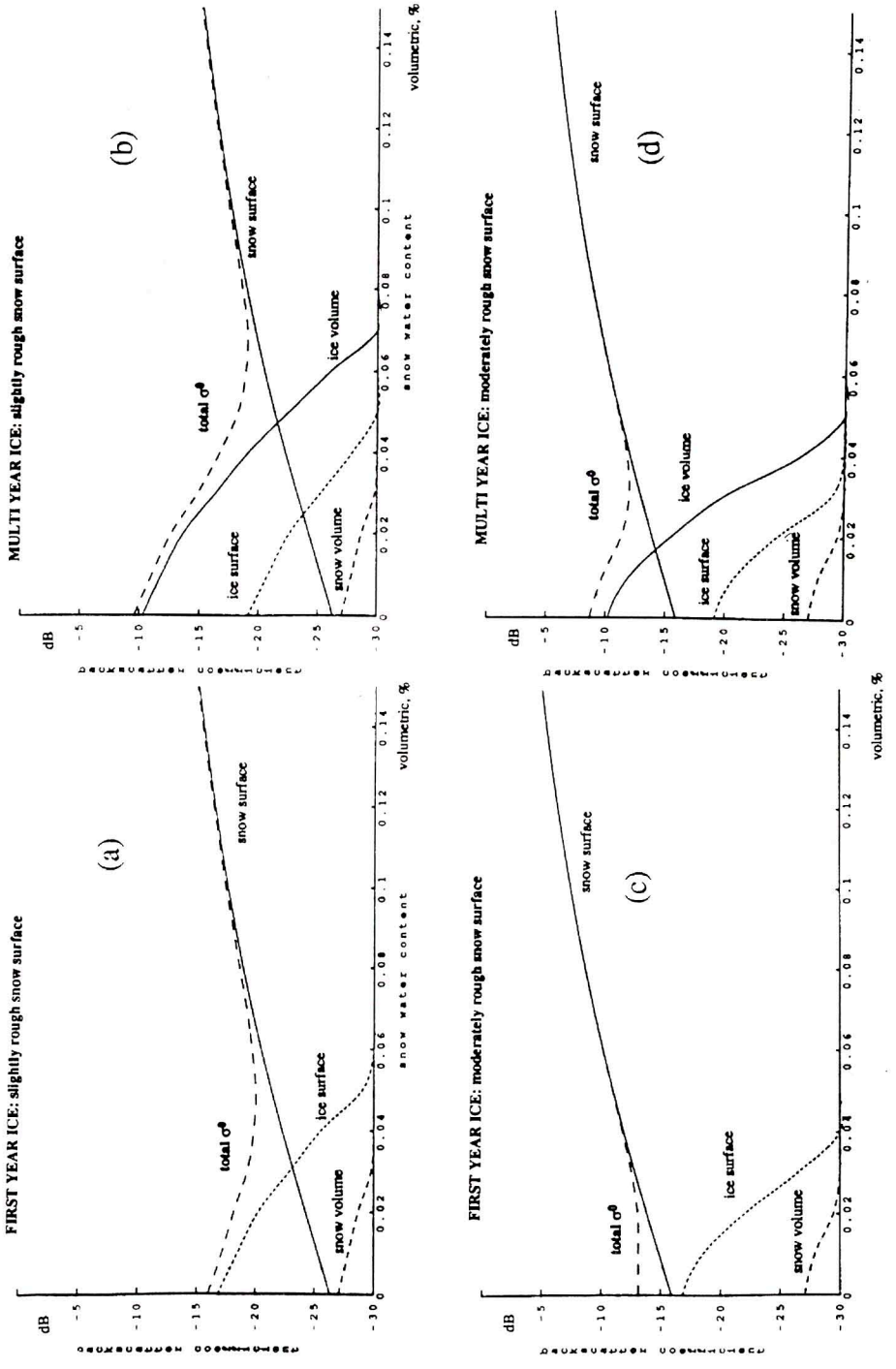

Fig. 8 - The backscatter coefficient from a snow-covered sea ice as a function of snow volumetric moisture content for ice and snow surface and volume scattering components. (a) top left - first-year ice with a slightly rough surface; (b) top right - multi-year ice with a slightly rough surface; (c) bottom left - first-year ice with a moderately rough surface; (d) bottom right - multi-year ice with a moderately rough surface

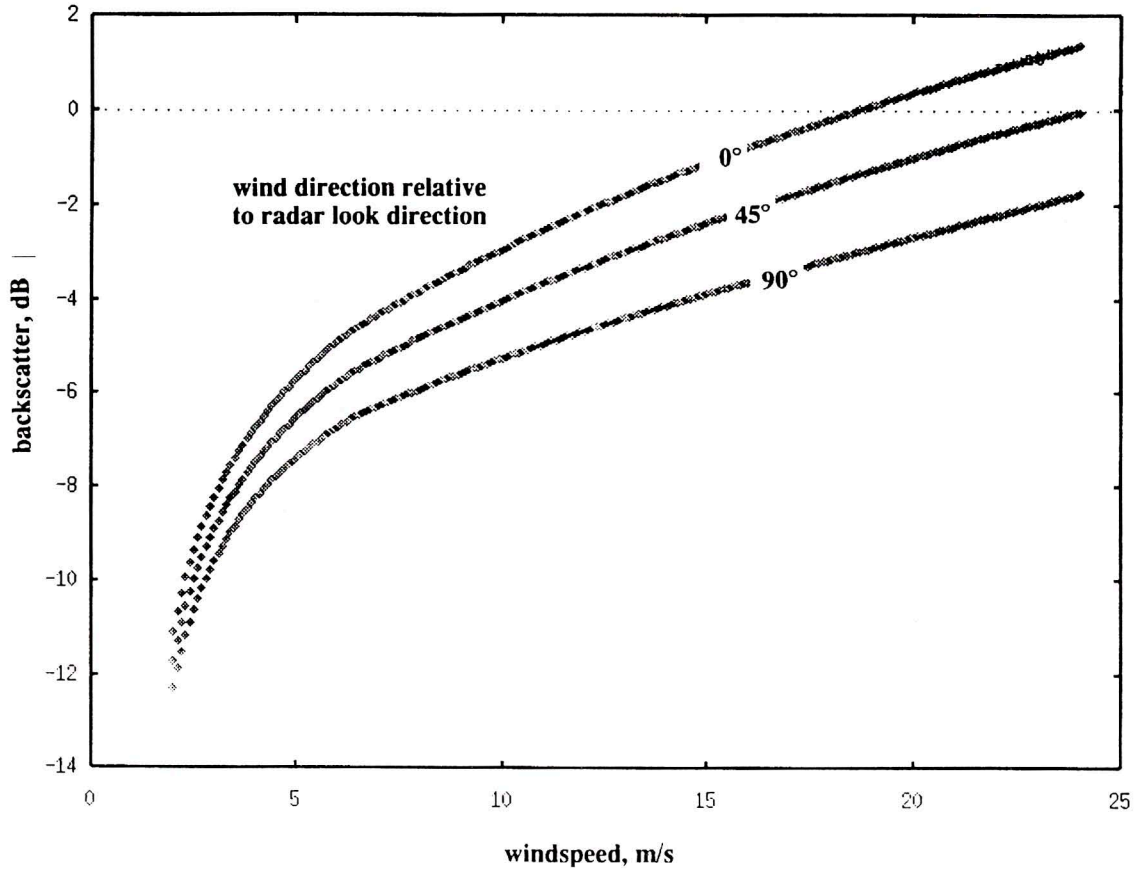

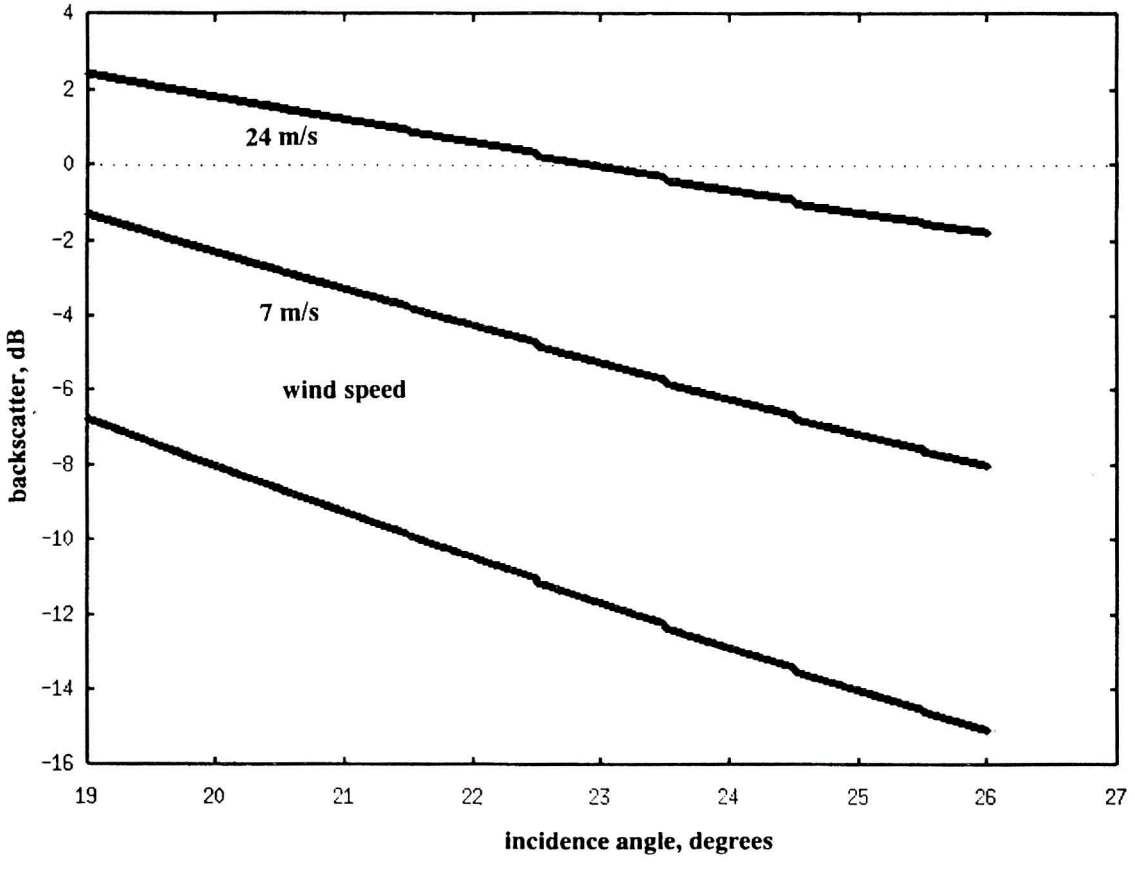

Fig. 9 - Predictions of the model CMOD4 for the backscatter coefficient from open water as a function of wind speed and direction (top, a) and incidence angle (bottom, b) (Lecomte, 1993)

intermediate wind speeds, significant over-prediction of ice concentration will occur.

There are a number of improvements to the model which would add to its realism. These are listed as follows:

(a) More detail on parameters are essential. The model is particularly limited by insufficient data on surface roughness related to different types and sea ice and snow.
(b) Snow scattering. Multiple reflections between the upper and lower surfaces of the snow may be significant. The model of snow layer is thought likely to be a weak part of the model. The assumption of far-field scattering of ice grains may well be violated.
(c) Ice scattering. Some systematic variation of properties with depth may be useful.

For the purposes of backscatter modelling, it is important to note that certain ice properties are less significant to scattering than others, as indicated in this paper, and so more data concentrated on those properties which are important would advance our ability to predict backscatter signatures and mechanisms for different types of ice.

7. ACKNOWLEDGEMENTS

This work was sponsored by the British National Space Centre via the DRA Aerospace Division, Farnborough, UK. The initial development of the backscatter model was funded by GEC-Marconi Ltd. ERS-1 data in support of the project has been provided by ESA. The authors would also like to thank the anonymous referees for useful comments.

8. REFERENCES

Ambach W. & Denoth A., 1980, "The dielectric behaviour of snow: a study versus liquid water content", No 25 in NASA Conf. Proc. 2153 (A. Rango ed.) Washington DC.

Cavalieri D.J. & Onstott R.G., 1992, 'Arctic coastal polynya observations with ERS-1 SAR and DMSP SSM/I", ESA SP-359, First ERS-1 Symposium, "Space at the service of our environment", Cannes, France, pp. 295-300.

Cunningham G., Kwok R & Holt B, 1992, "Preliminary results from the ASF/GPS ice classification algorithm", Proc. IGARSS '92, IEEE Publ., No. 92, CH3041-1, pp. 573-575.

de Loor G.P., 1968, "Dielectric properties of heterogeneous materials containing water", Journal Microwave Power, Vol. 3.

Drinkwater M.R., 1989, "Limex '87 ice surface characteristics: Implications for C band backscatter signatures, Trans. Geosci. Rem. Sens., Vol. 27, No 5.

Evans S., 1965, "Dielectric properties of ice and snow - a review", Glac., Vol. 5, No 42, pp. 782-783.

Fetterer F. & Gineris D., 1992, "ERS-1 SAR as a data source for operational ice analysis", ESA SP-359, First ERS-1 symposium, "Space at the service of our environment", Cannes, France, pp. 373-378.

Gogineni S.P., 1986, Radar backscatter from sea ice", IEEE National Radar Conference Proceedings, CH2270-7/86/0000-0107, pp. 107-114.

Hallikainen M. & Toikka M., 1992, "Classification of sea ice types with radar", Proc. 2nd European Microwave Conference '92, Espoo, Finland.

Hallikainen M., Ulaby F.T. & Abdelrazik M., 1986, "The dielectric properties of snow in the 3 to 37 GHz range", IEEE Trans. Ant. and Prop., Vol. AP-39, No 11, pp. 1329-1340.

Hoekstra P. & Spanogle D., 1972, "Radar cross-section measurements of snow and ice", US Army Corps of Engineers, CRREL, Hanover, NH, Technical Report 235.

Ishimaru A., 1978, "Wave propagation and scattering in random media", Vol. 1, pp. 12-25, publ. Academic Press Inc.,

Johannessen O.M., Sandven S., Campbell W.J. & Shuchman R., 1992, "ERS-1 SAR ice signature validation during SIZEX '92", ESA SP-359, First ERS-1 Symposium, "Space at the service of our environment", Cannes, France, pp. 277-282.

Kim Y-S, Moore R.K. & Onstott R.G., 1984, "Theoretical and experimental study of radar backscatter from sea ice", Remote Sensing Laboratory Technical Report RSL TR 331-37, University of Kansas.

Kim Y-S, Onstott R.G. & Moore R.K., 1984, "The effect of a snow cover on microwave backscatter from sea ice", IEEE Trans. Oc. Eng., Vol. OE-9, No 5, pp. 383-388.

Lamb J, 1946, "Measurements of the dielectric properties of ice", Trans. Faraday Soc., Vol. 42A.

Lamb J. & Turney, A., 1949, "The dielectric properties of ice at 1.25 cm. wavelength", Proc. Phys. Soc., Section B, Vol. 62, Part 4.

Lang R.H. & Saleh H.A., 1985, "Microwave inversion of leaf area and inclination angle distributions from backscatter data", IEEE Trans. Geosci. Re, Sens., GE-23, No. 5, 685-694.

Lecomte P., 1993, "CMOD4 model description", ESA ESRIN report, ER-TN-ESA-GP-1120, Issue 1.2.

Livingstone C.E. & Drinkwater M.R., 1991, "Springtime C band SAR backscatter signatures of Labrador Sea marginal ice: Measurements versus modelling predictions", IEEE Trans. Geosci. Rem. Sensing. Vol. 29, No 1.

Schiffer R. & Thielheim K.O., "Light scattering by dielectric needles and disks", Journal Appl. Phys. 50(4), 2476-2483.

Stogryn A., 1977, "Equations for calculating the dielectric constant of saline water", IEEE Trans. Micro. Theory Techn., MIT 19, 733-736.

Stratton J.A., 1941, "Electromagnetic theory", McGraw-Hill Book Co., New York, pp. 201-207.

Toikka M. & Hallikainen M., 1992, "Radar backscatter signatures of Baltic Sea ice", Proc. IGARSS '92, IEEE Publ., No 92, CH3041-1, pp. 1527-1529.

Ulaby F.T., Moore R.K. & Fung A.K., 1986, "Microwave remote sensing active and passive", Artech House, inc.

Ulander L.M.H., Askne J. & Johannessen B.O., 1992, "Calibrated ERS-1 SAR Signatures and video underflights over Arctic sea ice", Proc. IGARSS '92, IEEE Publ., No 92, CH3041-1, pp. 1536-1538.

Ulander L.M.H. & Carlström A., 1992, "C band backscatter signatures of old ice in the central Arctic", Proc. IGARSS '92, IEEE Publ., No 92, CH3041-1, pp. 958-960.

Vant M.R., Gray R.O., Ramseier R.O. & Makios V., 1974, "Dielectric properties of fresh and sea ice at 10 and 35 GHz, Journal Appl. Physics, Vol. 45, No 11.

Vant M.R., Ramseier R.O. & Makios V., 1978, "The complex dielectric constant of sea ice at frequencies in the range 0.1-40 GHZ", Journal Appl. Physics, Vol. 49, No 3, pp. 1264-1280.